INTERNATIONAL JOURNAL FOR NUMERICAL METHODS IN FLUIDS, VOL. 14, 1325–1345 (1992)

AN EXTENDED k–ε FINITE ELEMENT MODEL

MARC JAEGER

Université de Technologie de Compiègne, Compiègne, France

AND

GOURI DHATT

Université de Technologie de Compiègne, Department Genie Mecanique, BP 649-60206, Compiègne, Cedex, France and Université Laval, Québec, Canada

SUMMARY

An extended k–ε model (to include low-Reynolds-number regions) employing weighting functions is presented. Wall functions for the near-wall zones are developed giving correct boundary values for the shear stress and k–ε. A finite element model using a penalty formulation for incompressible turbulent flow is applied to solve a flow between two plates. Results with mesh boundaries situated in the near-wall region and at the wall are compared with measured values.

KEY WORDS k–ε Wall functions Finite element

1 INTRODUCTION

The design task of real life flows is a difficult undertaking since there exist no reliable tools for predicting correctly the complex flow patterns. We have detailed experimental data for only simple flows but any empirical generalization to complex geometries is mostly erroneous. A designer welcomes the arrival of numerical simulation packages which allow one to obtain a better understanding of the velocity, vorticity and pressure profiles. The numerical simulation field is young, active and highly promising owing to fast-computing developments.

Turbulent flows are represented by the Navier–Stokes and continuity equations if the influence of all fluctuations, large- and small-scale, is taken into account. However, the available computational tools are not capable of solving these equations since it is not possible to represent correctly the small-scale fluctuations which are essential for simulating turbulence effects.

For practical applications one is content to predict large-scale fluctuations, often referred to as averaged quantities. However, these quantities do not satisfy the Navier–Stokes equations and we know of no other set of equations which may be employed to predict the evolution of averaged quantities. The present-day research efforts are thus devoted to constructing a mathematical model in terms of large-scale fluctuations. In this model the influence of small-scale fluctuations, called the turbulence effect, is correctly included without defining the small-scale quantities. The modelling of turbulence effects requires skill, inspiration and a correct understanding of these fluctuations.

The finite element modelling of turbulent flows is still in the early stages of development. The averaging process in the context of finite element discretization (or finite-difference-like discretization) has led to large-eddy simulation (LES) models. The essential idea is that large fluctuations

0271–2091/92/111325–21$10.50

Received February 1991
Revised October 1991

are simulated by finite element approximations (grid-size eddies) and small eddies relative to the grid size are modelled by empirical relations.[1-9] This approach although quite promising, cannot be applied successfully to engineering problems owing to the limited computing capabilities of today.

In this study we have opted for the averaged Navier–Stokes equations using the Reynolds time-filtering or time-averaging technique, which requires a correct modelling of turbulence (the closure problem). Reynolds[10] manipulated the Navier–Stokes and continuity equations to obtain a set of equations having an extra term corresponding to averaged products of fluctuating velocity components (called Reynolds stresses). Reynolds was interested in statistically stationary flows obtained by time averaging. The role of products of spatial velocity fluctuations is not clear. It may be implicitly assumed that Reynolds stresses include all turbulence effects. The averaged equations may be associated with the ensemble average.[11] We consider an ensemble of statistically independent flows subjected to the same set of boundary and initial conditions. The quantities, measured at the same time and position for different flows, are averaged by simply adding the values and dividing by the number of flows. We assume that averaged quantities have large-scale spatial–temporal variations and that Reynolds stresses group all turbulence effects.

The closure problem is related to defining Reynolds stresses. Boussinesq may be considered the first researcher who attempted to model turbulence or effective shear stress resulting from cross-correlation of fluctuating velocities by introducing the concept of 'turbulent or eddy viscosity'. In 1877 he suggested that turbulent stresses could be replaced by the product of mean velocity gradients and turbulent viscosity.[12] One employs either an algebraic relation, one-equation or two-equation models to evaluate the eddy viscosity,[13-17] which is a property of the flow and not of the fluid. Some researchers have proposed Reynolds stress models which do not require an eddy viscosity concept.[18-23] The application of such models for three-dimensional flows is unrealistic owing to the availability of only limited computational resources.

In this study we have opted for a two-equation k–ε (turbulence kinetic energy and rate-of-dissipation energy) closure model to define the eddy viscosity for incompressible flows. One may remark that not much experience exists with k–ε finite element models when applied in near-wall regions. We start with a presentation of the standard k–ε model which is mainly valid in the turbulent region (far-wall zone). The near-wall effects are simulated through wall functions which give boundary conditions for points situated in the turbulent zone. However, this procedure is not well adapted for complex flows, since the condition that the boundary be in the turbulent zone cannot generally be respected rigorously. The equations of the model and the boundary conditions given by the wall functions are both erroneously applied in such a case. The aim of our study is to demonstrate that the use of an extended version of the k–ε model (low-Reynolds-number model) in combination with wall functions defined over the entire wall region is a much better choice. In Sections 4 and 5 an extended k–ε model is presented which is valid in the near-wall (low-Reynolds-number) and far-wall (high-Reynolds-number) zones. The appropriate choice of wall functions in the near-wall zones is discussed in detail. A finite element model employing the eight-node hexahedral element with continuous velocities and local pressure is presented in Section 6. The pressure is locally eliminated by employing the penalized form of the continuity equation. Surface elements to introduce wall stresses, k–ε conditions and pressure forces are discussed as well. A brief description of the solution strategy using a Newton-type method to solve for velocity, pressure, turbulence energy k and rate-of-dissipation energy ε is given in the same section. Finally we validate the model by simulating the turbulent flow between two plates. We investigate mainly the validity of the k–ε model to include low-Reynolds-number zones and various positions of near-wall boundary employing wall functions. The results are compared with those obtained from experimental measurements.

2. STANDARD k–ε MODEL OF TURBULENCE

The continuity equation for incompressible flows (density ρ = constant) is

$$\frac{\partial u_i}{\partial x_i}=0, \quad i=1, 2, 3 \text{ (sum over repeated index)}, \tag{1}$$

where u_i is the velocity component and x_i is the Cartesian co-ordinate.

The Navier–Stokes equations for the conservation of momentum are obtained by employing Newton's laws of motion.[24,25] It may be stated: the external forces exerted by the surroundings on the volume element are equal to the rate of increase of momentum in the volume plus the net rate of efflux of momentum out of the volume through its surface. The external forces are fluid stresses exerted on the surface and volume forces such as gravity force. We have

$$\frac{\partial \rho u_i}{\partial t}+\frac{\partial}{\partial x_j}(\rho u_i u_j)+\frac{\partial p}{\partial x_i}-\frac{\partial \tau_{ij}}{\partial x_j}-\rho F_i=0, \quad i,j=1, 2, 3, \tag{2}$$

where p is the pressure, τ is the symmetrical viscous stress tensor and ρF_i is the volume force, which is assumed zero. For Newtonian flows the viscous stresses are defined by

$$\tau_{ij}=\mu\left(\frac{\partial u_i}{\partial x_j}+\frac{\partial u_j}{\partial x_i}\right), \tag{3}$$

where μ is the fluid viscosity (N s m^{-2}). Equations (1)–(3) represent a laminar or turbulent fluid behaviour. However, a numerical simulation model for turbulent flows employing these equations would require very fine spatial and temporal discretization to capture correctly the interaction of large- and small-scale fluctuations. No present-day computational equipment has a capability for direct simulation of industrial flows. It is thus necessary to employ averaged versions of the Navier–Stokes equations where only large-scale fluctations are calculated. The influence of small-scale fluctuations is modelled in an approximate or empirical manner. In 1883 Reynolds suggested representing a quantity $f(x, t)$ as the sum of time-averaged quantity and a fluctuating term:[10]

$$f(x, t)=\bar{f}(x)+f'(x, t),$$

$$\bar{f}(x)=\langle f\rangle=\frac{1}{T}\int_{-T/2}^{T/2} f(x, \tau)\,\mathrm{d}\tau, \quad \langle f'\rangle=0. \tag{4}$$

We may represent Reynolds' filter in a more general form where $f(x, t)$ is considered as sum of large-scale fluctuations (representable on an observable scale) $\bar{f}(x, t)$ and small-scale fluctuations (non-observable scale) $f'(x, t)$:

$$f(x, t)=\bar{f}(x, t)+f'(x, t), \qquad \bar{f}(x, t)=\langle f\rangle. \tag{5}$$

Reynolds averaging may be thought of as lowpass filter where all small-scale fluctuations of time–space are eliminated. One associates the following properties with the Reynolds-averaging operation:[11]

$$\langle f'\rangle=0, \qquad \langle\bar{f}\rangle=\bar{f}, \tag{6}$$

$$\langle\bar{f}f'\rangle=0, \qquad \langle fg\rangle=\bar{f}\bar{g}+\langle f'g'\rangle. \tag{7}$$

Equation (7) represents the most important property of Reynolds averaging. In effect, we assume that the frequency spectrum of small-scale fluctuations is far away from that of large-scale fluctuations, i.e. no interaction exists between the two scales.

The averaged Navier–Stokes equations (1) and (2) become

$$\frac{\partial \bar{u}_i}{\partial x_i}=0, \qquad \frac{\partial \bar{u}_i}{\partial t}+\frac{\partial(\bar{u}_i\bar{u}_j)}{\partial x_j}+\frac{\partial}{\partial x_j}\left(R_{ij}-\frac{1}{\rho}\bar{\tau}_{ij}\right)+\frac{1}{\rho}\frac{\partial \bar{p}}{\partial x_i}=0, \quad i,j=1,2,3, \tag{8}$$

where ρ is assumed constant and the Reynolds stresses are defined by

$$R_{ij}=\langle u_i' u_j'\rangle, \qquad u_i'=u_i-\bar{u}_i, \qquad p'=p-\bar{p}. \tag{9}$$

We introduce the concept of turbulent or eddy viscosity which relates Reynolds stresses to spatial gradients of averaged velocities. Following Boussinesq's proposition in 1877,[12] one obtains

$$-R_{ij}=\nu_t\left(\frac{\partial \bar{u}_i}{\partial x_j}+\frac{\partial \bar{u}_j}{\partial x_i}\right)-\tfrac{2}{3}k\delta_{ij}, \tag{10}$$

where ν_t is the eddy viscosity ($m^2\,s^{-1}$), δ_{ij} is Kronecker's symbol and ρk is the mean kineitc energy of fluctuations or turbulence:

$$k=\tfrac{1}{2}\sum R_{ii}=\tfrac{1}{2}\langle u_1' u_1'+u_2' u_2'+u_3' u_3'\rangle. \tag{11}$$

Using equation (10), the closure problem of defining R_{ij} is reduced to obtaining an expression for the eddy viscosity. It is obvious that ν_t is not characteristic of the fluid but of the flow. From dimensional analysis[26] one may observe that the eddy viscosity is the product of a characteristic velocity $k^{1/2}$ and a characteristic length $k^{1\cdot5}/\varepsilon$,

$$\nu_t=\frac{\mu_t}{\rho}=C_\mu\frac{k^2}{\varepsilon}, \tag{12}$$

where C_μ is an empirical constant and $\rho\varepsilon$ is called the rate of mean turbulent viscous dissipation:[11,23]

$$\varepsilon=\nu\left\langle\frac{\partial u_i'}{\partial x_j}\frac{\partial u_i'}{\partial x_j}\right\rangle. \tag{13}$$

The two turbulent quantities k and ε satisfy the following transport relations at each point of the flow domain:

$$\frac{\partial k}{\partial t}+\bar{u}_i\frac{\partial k}{\partial x_i}-\frac{\partial}{\partial x_i}\left(\frac{\nu_t}{\sigma_k}\frac{\partial k}{\partial x_i}\right)-\nu_t S+\varepsilon=0, \tag{14}$$

$$\frac{\partial \varepsilon}{\partial t}+\bar{u}_i\frac{\partial \varepsilon}{\partial x_i}-\frac{\partial}{\partial x_i}\left(\frac{\nu_t}{\sigma_\varepsilon}\frac{\partial k}{\partial x_i}\right)-C_{\varepsilon1}\nu_t\frac{\varepsilon}{k}S+C_{\varepsilon2}\frac{\varepsilon^2}{k}=0, \tag{15}$$

with

$$S=\tfrac{1}{2}\left(\frac{\partial \bar{u}_i}{\partial x_j}+\frac{\partial \bar{u}_j}{\partial x_i}\right)^2, \quad i,j=1,2,3 \text{ (sum over repeated index).}$$

The standard values of the five empirical constants of the model are[13,15]

$$C_\mu=0\cdot09, \quad C_{\varepsilon1}=1\cdot44, \quad C_{\varepsilon2}=1\cdot92, \quad \sigma_k=1\cdot0, \quad \sigma_\varepsilon=1\cdot3.$$

The transport equations for k–ε (equations (14) and (15)) are obtained from the Navier–Stokes equations by assuming that the turbulence effects dominate at every point of the flow domain,[27,28] i.e. all viscous terms are neglected before the turbulence terms.

Thus the standard k–ε model is valid in regions where the viscous terms are small compared with the turbulence effects. It is not valid in the near-wall zones, which include the viscous and buffer sublayers. The popular approach is not to consider the near-wall zones and employ wall functions. However, this is not practical for complex flows and may lead to undesirable results in numerical implementation. The difficulties are related to locating the turbulent zone and the possibility of having an irregular near-wall surface boundary. A solution procedure for a numerical model will find the task of locating the mesh points in the turbulent zone during one iteration cycle highly impractical.

In the following section we discuss various assumptions related to near-wall zones and the criteria employed to position the turbulent zone.

3. NEAR-WALL ZONE

The following assumptions are introduced in the near-wall zone.

(i) The resultant shear stress τ_w in the plane parallel to the solid wall is the only dominant force.
(ii) The value of τ_w is assumed constant in the near-wall zone.
(iii) The zone is divided into three sublayers: viscous layer, buffer layer and turbulent layer.

The shear friction velocity is defined by

$$u^* = \sqrt{\left(\frac{\tau_w}{\rho}\right)} \quad (\mathrm{m\,s^{-1}}). \tag{16}$$

The non-dimensional distance y^+ normal to the wall is employed to characterize the wall region:

$$y^+ = \frac{yu^*}{\nu}, \qquad u^+ = \frac{u}{u^*}. \tag{17}$$

One may consider y^+ as the wall Reynolds number. The shear stress τ_w is assumed constant in the wall region, which extends from the wall ($y^+ = 0$) to $y^+ = 100$. This region is composed of three sublayers.

(i) Viscous sublayer ($0 \leqslant y^+ \leqslant 5$): in this region closest to the wall the turbulence effects are considered small relative to viscous terms. We have

$$\frac{\tau_w}{\rho} = \nu \frac{\partial u}{\partial y}, \quad \text{leading to } u^+ = y^+, \tag{18}$$

where u is the tangential velocity in the plane of the wall

(ii) Turbulent sublayer ($30 \leqslant y^+ \leqslant 100$): in this region farthest from the wall the viscous terms are small relative to turbulence effects:

$$\frac{\tau_w}{\rho} = \nu_t \frac{\partial u}{\partial y}$$

By employing the mixing length expression

$$\nu_t = (\chi y)^2 \left|\frac{\partial u}{\partial y}\right|, \quad \text{with } \chi = 0{\cdot}4, \tag{19}$$

we obtain for a smooth wall[11]

$$u^+ = 2{\cdot}5 \ln y^+ + 5{\cdot}5. \tag{20}$$

(iii) Transition or buffer zone ($5 \leqslant y^+ \leqslant 30$): in this intermediate region both viscous and turbulence effects are present. The velocity profile is assumed logarithmic and the coefficients are adjusted to define a continuous velocity field in the complete wall zone. For a smooth wall we obtain

$$u^+ = 5{\cdot}0 \ln y^+ - 3{\cdot}05 \tag{21}$$

Thus the law of the wall (constant shear stress) allows us to determine the shape of the velocity profile in the wall region ($y^+ \leqslant 100$).

As mentioned earlier, the standard k–ε model cannot be used very near the wall. However, boundary layer flows can be treated by matching the high-Reynolds-number flow with the law-of-the-wall profile at the first grid point away from the wall. The point's distance from the wall should not be too large in order to lie inside the wall region ($y^+ \leqslant 100$), but also not small in order that the equations of the model remain valid ($y^+ \geqslant 30$). In other words, the point must be in the turbulent layer.

The shear stress condition applied at this point is deduced from (20):

$$\frac{\tau_w}{\rho} = (u^*)^2 = \left(\frac{u}{2{\cdot}5 \ln y^+ + 5{\cdot}5} \right)^2. \tag{22}$$

The boundary conditions for k and ε can be found using the assumption that dissipation equals production in the turbulent zone:

$$k = \frac{(u^*)^2}{\sqrt{C_\mu}}, \qquad \varepsilon = \frac{(u^*)^3}{\chi y}. \tag{23}$$

This procedure is generally known as the wall function technique.

Now, for complex flows, ensuring that each boundary grid point stands in the turbulent layer can become quite a tedious task, since the friction velocity can vary very rapidly for such flows. Moreover, the real position y of the boundary may become highly irregular. It is expected that updating the near-wall points will involve important oscillations of mesh positions and the strategy is not adaptable for practical situations.

This difficulty can be overcome by using a low-Reynolds-number k–ε model, which is valid up to the wall. The computation can then cover the enitre flow domain, including buffer and viscous zones. However, the computational cost would be much higher, since a very fine grid is needed for the wall region because of the very steep gradients one finds there.

The aim of the present study is to demonstrate that both approaches can be coupled to obtain a method no more expensive than the classical one but which does not suffer from the limitations we have mentioned earlier. The idea is to select an extended k–ε model as easy to implement as the standard one and to develop wall functions which are valid over the whole wall region, including buffer and viscous layers. Positioning the boundary is then an easy task, since the only condition to satisfy is to stay in the wall region. Of course, a computation up to the wall is within the scope of such a model.

4. EXTENDED k–ε MODEL

The averaged Navier–Stokes equations are valid in the near-wall (low-Reynolds-number) and far-wall (high-Reynolds-number) regions since the viscous and turbulent terms are retained

(equation (8), $\bar{\tau}_{ij}$ and R_{ij}). Extension of the k-equation to the low-Reynolds-number zone requires simply that the viscous term $\nu\partial k/\partial x_j$ be added to equation (14). However, extension of the ε-equation (equation (15)) to the near-wall region is not so straightforward, since ε does not tend to zero as one approaches the wall as is the case with the velocity and k-terms. It may be mentioned that ε equals the rate of mean turbulent viscous dissipation in the high-Reynolds-number region only.

The extension is possible by introducing three weighting functions $f_\mu, f_{\varepsilon 1}$ and $f_{\varepsilon 2}$ for the three constants C_μ, $C_{\varepsilon 1}$ and $C_{\varepsilon 2}$. Using these weighting functions, equations (12), (14) and (15) become

$$\nu_t = C_\mu f_\mu \frac{k^2}{\varepsilon}, \qquad \frac{\partial k}{\partial t} + \bar{u}_i \frac{\partial k}{\partial x_i} - \frac{\partial}{\partial x_i}\left[\left(\frac{\nu_t}{\sigma_k} + \nu\right)\frac{\partial k}{\partial x_i}\right] - \nu_t S + \varepsilon = 0, \tag{24}$$

$$\frac{\partial \varepsilon}{\partial t} + \bar{u}_i \frac{\partial \varepsilon}{\partial x_i} - \frac{\partial}{\partial x_i}\left[\left(\frac{\nu_t}{\sigma_\varepsilon} + \nu\right)\frac{\partial \varepsilon}{\partial x_i}\right] - C_{\varepsilon 1} f_{\varepsilon 1} \nu_t \frac{\varepsilon}{k} S + C_{\varepsilon 2} f_{\varepsilon 2} \frac{\varepsilon^2}{k} = 0.$$

The weighting functions depend on the local Reynolds numbers in the near-wall zone, which are defined by

$$R_t = \frac{k^2}{\nu\varepsilon}, \qquad R_y = \frac{\sqrt{(k)}\, y}{\nu} \tag{25}$$

In References 27 and 29–34 different expressions for the weighting functions are suggested which are related to the extended k–ε model (also called the low-Reynolds-number model). Our numerical experimentation permits us to retain the following expressions for $f_{\varepsilon 1}$ and $f_{\varepsilon 2}$:

$$f_{\varepsilon 1} = 1 + \left(\frac{A_{\varepsilon 1}}{f_\mu}\right)^3, \qquad f_{\varepsilon 2} = 1 - A_{\varepsilon 2} \exp\left[-(B_{\varepsilon 2} R_t)^2\right], \tag{26}$$

where $A_{\varepsilon 1}$, $A_{\varepsilon 2}$ and $B_{\varepsilon 2}$ are numerical constants.

The choice of f_μ is quite important for obtaining the desired results. Patel *et al.*[35] have discussed this aspect on the basis of a comparison of seven low-Reynolds-number models with experimental results. It turns out that none of the suggested expressions for f_μ behaves correctly. Two of them, however, seem more satisfactory than the others, namely Launder and Sharma,[29]

$$f_\mu = \exp\left(-\frac{A_\mu}{(1 + B_\mu R_t)^2}\right), \tag{27}$$

and Lam and Bremhorst,[33]

$$f_\mu = [1 - A_\mu \exp(-B_\mu R_y)]^2 \left(1 + \frac{D_\mu}{R_t}\right), \tag{28}$$

where A_μ, B_μ and D_μ are numerical constants.

By calculating the individual terms of the exact transport equations for k and ε using direct simulation data, Miner *et al.*[36] have found that the production term is the term most affected by changes in the wall damping function. From a comparison of this term (k-equation), calculated from direct simulation data and that modelled with f_μ, it appears that the Lam–Bremhorst expression gives best agreement.[36]

In the extended model of equations (24) one must ensure that no term goes to infinity as k approaches zero in the near-wall region. By choosing $A_{\varepsilon 2} = 1$ in (26), the singular term $f_{\varepsilon 2}\varepsilon^2/k$ approaches zero as k becomes small.

The determination of a correct boundary condition for ε is essential for obtaining reliable results with the extended model. An insight into the proper choice of ε-value is obtained by

employing a Taylor series development of k and ε near the wall. To start, we express the in-plane fluctuating components u' and w' and the normal component v' in terms of the wall distance y(x–z is the wall plane and y the normal direction):

$$u'(y)=a_1 y+a_2 y^2, \qquad v'(y)=b_2 y^2, \qquad w'(y)=c_1 y+c_2 y^2. \tag{29}$$

These relations satisfy the no-slip condition. The coefficients $a_1, a_2, \ldots$ are functions of x, z and t and the velocity is assumed to satisfy the incompressibility constraint. The expressions for k and ε are

$$k=\tfrac{1}{2}\langle u'^2+v'^2+w'^2\rangle=Ay^2+By^3+\ldots, \quad \varepsilon=\nu\left\langle\frac{\partial u_i'}{\partial x_j}\frac{\partial u_i'}{\partial x_j}\right\rangle=2\nu(A+2By+\ldots), \tag{30}$$

with

$$A=\frac{a_1^2+c_1^2}{2}, \qquad B=a_1a_2+c_1c_2.$$

It is possible to define different variants of the boundary condition for ε which satisfy (30). In References 31 and 33 a condition is employed which is difficult to implement in finite element modelling, namely

$$\varepsilon_{y=0}=\nu\left(\frac{\partial^2 k}{\partial y^2}\right)_{y=0} \tag{31}$$

Patel *et al.*[35] employ a simpler condition

$$\left(\frac{\partial\varepsilon}{\partial y}\right)_{y=0}=0, \quad \text{leading to } B=0. \tag{32}$$

However, the simulation of Chapman and Kuhn[37] tends to invalidate the choice of $B=0$. They suggested the following expression:

$$\varepsilon_{y=0}=\left(4\nu\frac{k}{y^2}-\varepsilon\right)_{y=\text{small distance}}. \tag{33}$$

This condition is easy to implement and leads to stable results.

In summary, the extended model is defined by equations (24) along with the weighting functions given by equations (26)–(28). This model is valid up to the wall and the boundary condition for ε on the wall is given by equation (33). In the following section we present appropriate wall functions which allow us to position the flow domain in the near-wall zone, leading to important computational savings.

5. CHOICE OF WALL FUNCTIONS

The extended k–ε model allows us to simulate the flow behaviour in the complete wall region extended to the wall. However, it is a costly option since one requires an extremely fine mesh in the wall region. It is preferable if the flow domain is not fully extended to the wall but is limited to near-wall zones. One then requires the boundary conditions on shear stress, k and ε for points situated in this zone. These conditions must be compatiable with the positions of points, which may lie in the viscous, buffer or turbulent sublayer. We present an extension to wall functions which are valid for the complete wall region.

Assuming the boundary points are situated in the wall region, the sublayer associated with a point is obtained by calculating y^+ from (17). The corresponding value of τ_w is easily calculated from equation (18), (20) or (21) in terms of u (see equation (22) for the turbulent layer).

For the conditions of k and ε one cannot employ equations (23) for points near the wall. For small y^+ one would obtain a non-zero value of k and a large value for ε which is not acceptable. The correct behaviour of k and ε near the wall is obtained from series expansion of equations (30). By retaining terms up to y^2 for k and ε with $B=0$, we have

$$k=Ay^2=A\frac{v^2}{(u^*)^2}(y^+)^2, \qquad \varepsilon=2vA+Cy^2=2vA+\frac{Cv^2}{(u^*)^2}(y^+)^2. \tag{34}$$

The coefficients A and C are determined by equating the values of k and ε to those defined by equations (23) at some non-dimensional distance δ from the wall:

$$k(y^+=\delta)=\frac{Av^2}{(u^*)^2}\delta^2=\frac{(u^*)^2}{\sqrt{C_\mu}}, \qquad \varepsilon(y^+=\delta)=2vA+\frac{Cv^2}{(u^*)^2}\delta^2=\frac{(u^*)^4}{\chi v\delta}. \tag{35}$$

Solving equations (35), we obtain

$$A=\frac{(u^*)^4}{v^2\delta^2\sqrt{C_\mu}}, \qquad C=\frac{(u^*)^6}{v^3\delta^3}\left(\frac{1}{\chi}-\frac{2}{\delta\sqrt{C_\mu}}\right). \tag{36}$$

When a point is situated in the zone $y^+\geqslant\delta$, equations (23) define the values of k and ε. For $y^+\leqslant\delta$ we chose

$$k=\frac{(u^*)^2}{\sqrt{C_\mu}}\left(\frac{y^+}{\delta}\right)^2, \qquad \varepsilon=\frac{(u^*)^4}{v\delta\chi}\left\{\left(\frac{y^+}{\delta}\right)^2+\frac{2\chi}{\delta\sqrt{C_\mu}}\left[1-\left(\frac{y^+}{\delta}\right)^2\right]\right\}. \tag{37}$$

The experimental results suggest $8\leqslant\delta\leqslant12$.

In Table I various aspects of the extended or low-Reynolds-number k–ε model are summarized. In Figure 1 we present the standard k–ε conditions (equations (23)) and the proposed k–ε conditions (equations (37)) for the complete wall zone. The non-dimensional quantities $k^+=k/(u^*)^2$ and $\varepsilon^+=\varepsilon v/(u^*)^4$ are plotted against y^+.

6. FINITE ELEMENT MODEL

For finite element applications we employ the stationary version of the k–ε model. All quantities are used in the non-dimensional form

$$x_i=\frac{x_i}{L}, \qquad u_i=\frac{\bar{u}_i}{V}, \qquad p=\frac{\bar{p}}{\rho V^2}, \qquad \tau_{ij}=\frac{\bar{\tau}_{ij}-\rho R_{ij}}{\rho V^2}, \qquad k=\frac{k}{V^2}, \qquad \varepsilon=\frac{\varepsilon L}{V^3}, \tag{38}$$

where L and V are the large-scale characteristic length and velocity respectively. The complete system of equations, with the incompressibility constraint in a penalty form, is written as

$$\frac{\partial}{\partial x_j}(u_ju_j+p\delta_{ij}-\tau_{ij})=0, \quad \frac{\partial u_j}{\partial x_j}-\frac{p}{\lambda}=0, \quad i,j=1,2,3 \text{ (sum over repeated index)}, \tag{39}$$

$$\frac{\partial}{\partial x_j}(u_jk+q_{kj})+E_k=0, \qquad \frac{\partial}{\partial x_j}(u_j\varepsilon+q_{\varepsilon j})+E_\varepsilon=0,$$

Table I Extended k–ε model

Non-dimensional quantities:

$$u^*=\sqrt{\left(\frac{\tau_w}{\rho}\right)}, \qquad y^+=\frac{yu^*}{\nu}, \qquad u^+=\frac{u}{u^*}, \qquad k^+=\frac{k}{(u^*)^2}, \qquad \varepsilon^+=\frac{\varepsilon\nu}{(u^*)^4}$$

Average Navier–Stokes equations:

$$\frac{\partial\bar{u}_i}{\partial x_i}=0, \qquad \frac{\partial\bar{u}_i}{\partial t}+\frac{\partial}{\partial x_j}(\bar{u}_i\bar{u}_j+R_{ij}+\bar{p}\delta_{ij}-\bar{\tau}_{ij})=0, \qquad -R_{ij}=\nu_t\left(\frac{\partial\bar{u}_i}{\partial x_j}+\frac{\partial\bar{u}_j}{\partial x_i}\right)-\tfrac{2}{3}k\delta_{ij}$$

k–ε extented relations:

$$\nu_t=\frac{C_\mu f_\mu k^2}{\varepsilon}, \qquad \frac{\partial k}{\partial t}+\bar{u}_i\frac{\partial k}{\partial x_i}-\frac{\partial}{\partial x_i}\left[\left(\frac{\nu_t}{\sigma_k}+\nu\right)\frac{\partial k}{\partial x_i}\right]-\nu_t S+\varepsilon=0$$

$$\frac{\partial\varepsilon}{\partial t}+\bar{u}_i\frac{\partial\varepsilon}{\partial x_i}-\frac{\partial}{\partial x_i}\left[\left(\frac{\nu_t}{\sigma_\varepsilon}+\nu\right)\frac{\partial\varepsilon}{\partial x_i}\right]-C_{\varepsilon1}f_{\varepsilon1}\nu_t\frac{\varepsilon}{k}S+C_{\varepsilon2}f_{\varepsilon2}\frac{\varepsilon^2}{k}=0$$

$f_{\varepsilon1}, f_{\varepsilon2}$, and f_μ given by equations (26)–(28)

Boundary conditions in near-wall zone: τ_w, equation (18) ($0\leqq y^+\leqq 5$), equation (20) ($5\leqslant y^+\leqslant 30$) or equation (21) ($30\leqslant y^+\leqslant 100$); k and ε, equations (23) ($y^+\geqslant\delta$) equations (37) ($y^+\leqslant\delta$) with $8\leqslant\delta\leqslant 12$

Boundary conditions on wall: $u_1, k=0$; ε, equation (33)

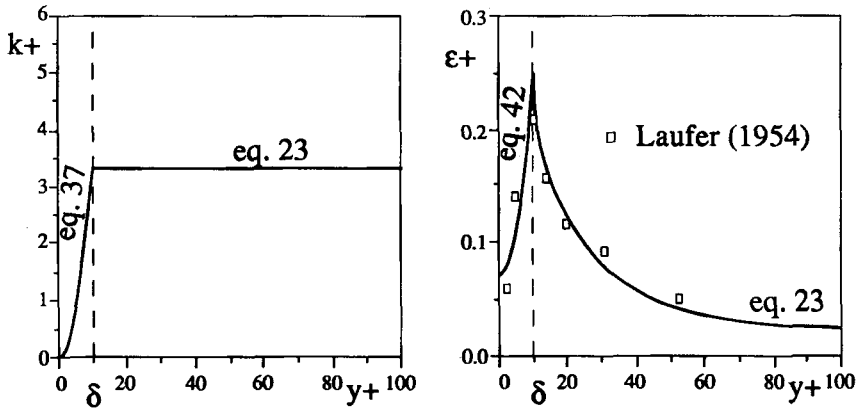

Figure 1. Near-wall k–ε boundary conditions

with

penalty coefficient $\lambda\approx 10^8$, shear flux $\tau_{ij}=\left(\frac{1}{R_e}+\frac{1}{R_{et}}\right)\left(\frac{\partial u_i}{\partial x_j}+\frac{\partial u_j}{\partial x_i}\right)$,

k-flux $q_{kj}=-\left(\frac{1}{R_e}+\frac{1}{\sigma_k R_{et}}\right)\frac{\partial k}{\partial x_j}$, ε-flux $q_{\varepsilon j}=-\left(\frac{1}{R_e}+\frac{1}{\sigma_\varepsilon R_{et}}\right)\frac{\partial\varepsilon}{\partial x_j}$,

k-production dissipation $E_k=-\frac{1}{R_{et}}S+\varepsilon$, $S=\frac{1}{2}\left(\frac{\partial u_i}{\partial x_j}+\frac{\partial u_j}{\partial x_i}\right)^2$,

ε-production dissipation $E_\varepsilon=-C_\mu f_\mu C_{\varepsilon1}f_{\varepsilon1}kS+C_{\varepsilon2}f_{\varepsilon2}\frac{\varepsilon^2}{k}$.

The weighting functions $f_\mu, f_{\varepsilon 1}$ are $f_{\varepsilon 2}$ are given by equations (26)–(28) and the five constants are $C_\mu = 0{\cdot}09$, $C_{\varepsilon 1} = 1{\cdot}44$, $C_{\varepsilon 2} = 1{\cdot}92$, $\sigma_k = 1{\cdot}0$ and $\sigma_\varepsilon = 1{\cdot}3$. The different Reynolds numbers are

$$R_e = \frac{VL}{\nu}, \quad \frac{1}{R_{et}} = C_\mu f_\mu \frac{k^2}{\varepsilon} = \nu_t \quad (k, \varepsilon, y \text{ in non-dimensional form}), \quad R_t = R_e \frac{k^2}{\varepsilon}, \quad R_y = R_e y \sqrt{k}. \tag{40}$$

The weak Galerkin variational form is given as[38]

$$W_{NS} = \int_\Omega \left[\delta u_i \frac{\partial}{\partial x_j}(u_i u_j) + \delta e_{ij}(\tau_{ij} - p\delta_{ij}) + \delta p \left(\frac{\partial u_j}{\partial x_j} - \frac{p}{\lambda} \right) \right] d\Omega$$
$$- \int_S (\delta \tilde{u}_t \vec{f}_t + \delta u_n f_n)\, dS = 0 \quad \forall \delta u_i, \delta p, \tag{41}$$

$$W_{k\varepsilon} = \int_\Omega \left[\delta\varepsilon \left(\frac{\partial}{\partial x_j}(k u_j) + E_k \right) - \frac{\partial \delta k}{\partial x_j} q_{kj} + \delta\varepsilon \left(\frac{\partial}{\partial x_j}(\varepsilon u_j) + E_\varepsilon \right) - \frac{\partial \delta\varepsilon}{\partial x_j} q_{\varepsilon j} \right] d\Omega$$
$$+ \int_S (\delta k q_{kn} + \delta\varepsilon q_{\varepsilon n})\, dS = 0 \quad \forall \delta k, \delta\varepsilon \tag{42}$$

where δu_i, δp, δk and $\delta\varepsilon$ are the Galerkin-type test functions, $\delta e_{ij} = \frac{1}{2}(\partial \delta u_i/\partial x_j + \partial \delta u_j/\partial x_i)$, f_n and $\vec{f}_t$ are the normal and tangential forces at the appropriate boundary respectively and q_{kn} and $q_{\varepsilon n}$ are the normal k- and ε-flux respectively.

We employ an eight-node hexahedral element (Figure 2) with a C^0-approximation for velocity components u_i and k–ε. The pressure is assumed constant over each element and is eliminated at the element level. Although this element does not satisfy the LBB conditions of stability, it gives good results for smooth boundary conditions.[39]

In our study we have considered either Neumann or Dirichlet boundary conditions for k–ε; thus the surface integrals in $W_{k\varepsilon}$ are zero. The surface terms in W_{NS} are useful in imposing pressure gradients via f_n and wall shear stress via $\vec{f}_t$. We have developed a special four-node surface element (Figure 3) with three velocity components u_i as variables. This element is employed to introduce either the pressure value or the tangential stress on the near-wall boundaries with normal velocity considered zero.

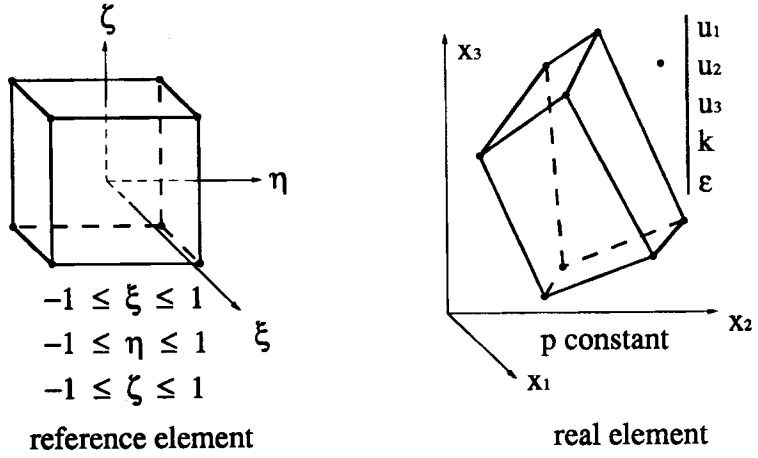

Figure 2. Hexahedral element

Finite element discretization yields a non-linear system of equations for u_i, k, and ε. We employ a solution strategy where the Navier–Stokes and k–ε equations are solved in a decoupled manner. A Newton-type method is used to solve each set of equations. The Reynolds number R_e in all diffusion terms is progressively increased from laminar to real flow values. This is achieved by progressively increasing the value of a relaxation coefficient α from a small value to unity in the following terms:

$$\tau_{ij}=\left(\frac{1}{\alpha R_e}+\frac{1}{R_{et}}\right)\left(\frac{\partial u_i}{\partial x_j}+\frac{\partial u_i}{\partial x_j}\right), \quad q_{kj}=\left(\frac{1}{\alpha R_e}+\frac{1}{\sigma_k R_{et}}\right)\frac{\partial k}{\partial x_j}, \quad q_{\varepsilon j}=\left(\frac{1}{\alpha R_e}+\frac{1}{\sigma_\varepsilon R_{et}}\right)\frac{\partial \varepsilon}{\partial x_j}. \tag{43}$$

During the early stages any appearances of negative values of k and ε are flagged to zero. One also employs an underrelaxation coefficient for the iteration update of k and ε. Different aspects of the solution strategy are summarized in Table II.

7. VALIDATION

In this study we have limited ourselves to the validation of the extended model applied to a flow between two plates. This flow has been experimentally studied by Comte-Bellot.[40] The numerical simulation with 17 different computations is undertaken to investigate different aspects:

(i) performance of low-Reynolds-number k–ε model with ε-boundary condition of Chapman and Kuhn[37] (equation (33)); the mesh is extended up to the wall
(ii) performance of the model employing wall functions (equation (18), (20) or (21) for τ_w and equations (23) or (37) for k and ε) with the mesh boundary situated at differents positions in the near-wall zone ($0 \leqslant y \leqslant 0{\cdot}05$)
(iii) assess the influence and precision of weighting functions f_μ, $f_{\varepsilon 1}$ and $f_{\varepsilon 2}$ (equations (26)–(28)) for different near-wall mesh positions
(iv) assess the influence of inflow and outflow boundary conditions, especially the pressure differential conditions and Neuman condition on k–ε
(v) identify certain aspects of solution strategy which will be employed for capturing complex flows.

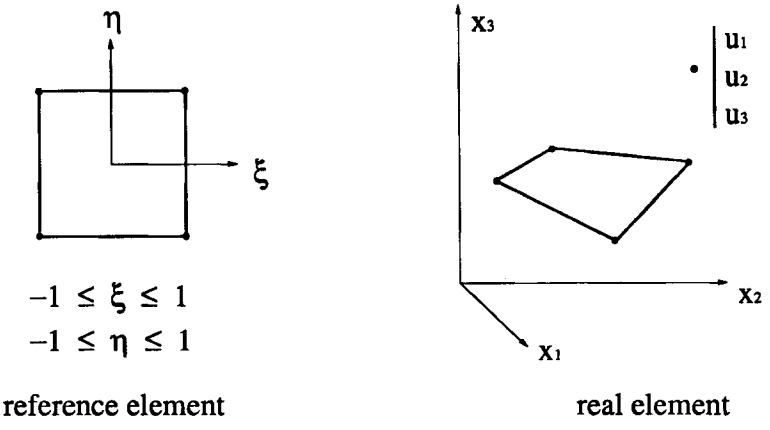

Figure 3. Quadrilateral boundary element

Table II. Solution strategy

*Select initial solution: $\{u_0\}$, $\{k_0\}$, $\{\varepsilon_0\}$

– Obtain laminar solution with low R_e: $\{u_0\}$
– Obtain $\{k_0\}$, $\{\varepsilon_0\}$ with $\{u_0\}$ and production–dissipation terms set to zero

*Solution phase—incremental Reynolds number update strategy

- For each $\alpha=\alpha_0, \alpha_1, \ldots, 1$: $R_e=\alpha R_e$
  - k–ε solution phase
    - Update boundary conditions
    - Solve for k–ε
    - Update: $\{k\}=\{k\}+\omega\{k\}$; $0\leqslant\omega\leqslant 1$
      $\{\varepsilon\}=\{\varepsilon\}+\omega\{\Delta\varepsilon\}$
    - Flag negative k, ε to zero
  - NS solution phase
    - Update eddy viscosity. Employ a smoothing if necessary
    - Solve non-linear equations. Iterate if necessary
    - Update: $\{u\}=\{u\}+\{\Delta u\}$
  - Repeat k–ε and NS phases till convergence

  Solve for a new value of α

* Evaluate required quantities: pressure field, shear stress, vortex field, etc.

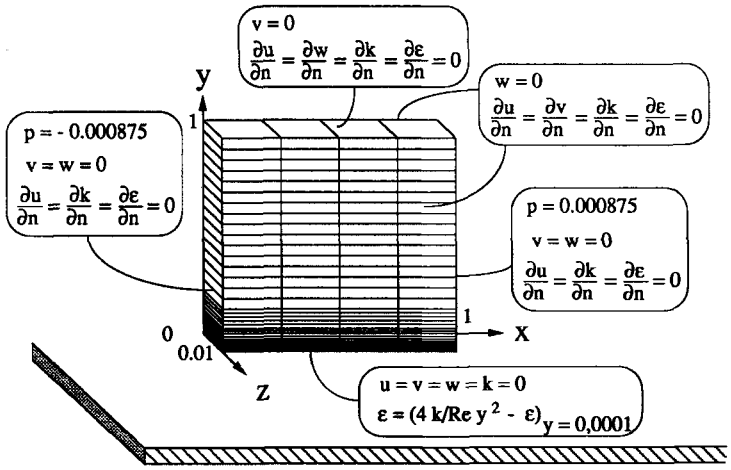

Figure 4. Near-wall k–ε boundary conditions

A mesh of $4\times71\times1$ elements is employed to discretize a geometry of $1\times1\times0{\cdot}01$ as shown in Figure 4. The wall is situated at $y=0$ and symmetry conditions are employed along five faces. The flow corresponds to a Reynolds number of 63 000 (Compte-Bellot obtains $Re=57\,000$ for the same flow with a velocity $V=10{\cdot}5\ \mathrm{m\,s^{-1}}$ at the centre and a canal half-width of 0·09 m). Since the flow quantities vary basically along the y-direction, we have employed one layer along the transverse z-direction and four layers of elements along the flow direction. It must be noted that with elements of greater size in the transverse direction (z-direction) we have found some difficulites in obtaining convergence. It appeared that the k–ε system was very sensitive to a small

lack of symmetry of the solution in the transverse direction due to round-off errors. The minimum size of element along the y-direction is 0·0001 near the wall and 0·05 at the centre.

A pressure gradient of 0·0175 is imposed along the inflow and outflow faces as shown in Figure 4. Comte-Bellot reported a pressure gradient of 0·0150, which underestimated the flow in our simulation. All quantities are in normalized or non-dimensional form. Special boundary elements are employed to introduce a pressure condition which results in equivalent load vectors. It is found that the pressure condition is quite efficient and avoids the necessity of introducing the correct velocity profile as inlet condition. Otherwise a large number of elements along the x-direction may be required, which could become undesirable.

The weighting functions $f_{\varepsilon 1}$ and $f_{\varepsilon 2}$ defined by equations (26) are shown in Figure 5 with $A_{\varepsilon 1} = 0{\cdot}05$ and $A_{\varepsilon 2} = B_{\varepsilon 2} = 1$. The function f_μ proposed by Launder and Sharma (equation (27)) has given erroneous results for our study. This is in agreement with the study of Miner *et al.*,[36] which has shown that the damping function f_μ proposed by Lam and Bremhorst[33] gives better results

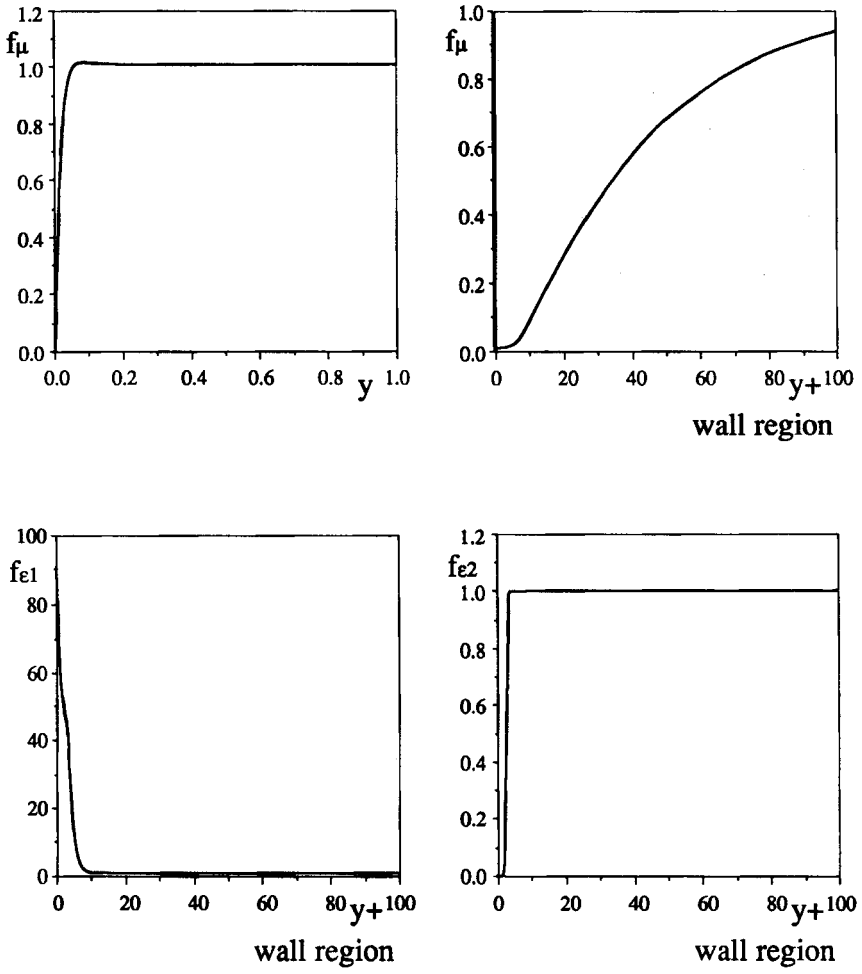

Figure 5. Weighting functions f_μ, $f_{\varepsilon 1}$ and $f_{\varepsilon 2}$

than that of Launder and Sharma.[29] We retained f_μ (equation (28)) proposed by Lam and Bremhorst with $B_\mu = 0{\cdot}0165$, $D_\mu = 20{\cdot}5$ and $A_\mu = 1$. The behaviour of f_μ is shown in Figure 5.

7.1. *Reference computation*

The reference computation represents the simulation of the flow with the mesh extended to the wall (Figure 4). We consider this computation as a basis for comparing the results obtained with the mesh boundary situated in different positions of the near-wall zone.

At the wall the velocity components u_1, u_2, u_3 and k are set to zero. The condition for the rate-of-dissipation energy ε is defined by equation (33):

$$\varepsilon_{y=0} = \left(\frac{4}{R_e} \frac{k}{y^2} - \varepsilon \right)_{y=0{\cdot}001}. \tag{44}$$

A special strategy as described below is required to obtain a convergent solution even for such a simple flow, since inflow and outflow conditions are only related to pressure (no velocity or k–ε profiles are prescribed).

Phase 1. Initial estimates for velocity and k–ε

1. Choose $v = w = 0$ and flowwise velocity $u = u_w$ at the wall boundary. The Reynolds number is determined so that an almost plane profile is obtained with laminar calculations:

   $R_e = 8$ and $u_w = 0{\cdot}7$, leading to $0{\cdot}7 \leqslant u(y) \leqslant 0{\cdot}707$.

   Solve the Navier–Stokes equations.
2. The k–ε system is solved by setting the production–dissipation terms E_k and E_ε (equations (39)) to zero with the velocity field of step 1. At the wall k_w and ε_w are set to a non-zero value ($k_w = 2\varepsilon_w$) such that the effective Reynolds number is equal to $R_e = 8$ of step 1:

$$\frac{1}{6300} + C_\mu \frac{k_w^2}{\varepsilon_w} = \frac{1}{8}$$

3. Start the decoupled resolution of the NS system and k–ε systems. During this stage gradually relax k_w and $\varepsilon_w (k_w = 2\varepsilon_w)$ until $\varepsilon_w = 0{\cdot}01$. The value of u_w remains fixed at 0·7 (about 50 iterations).

Phase 2. Relaxation of u_w and k_w to zero

1 Solve the decoupled system by slowly relaxing u_w and k_w to zero, keeping $\varepsilon_w = 0{\cdot}01$ (about 40 iterations).
2. Obtain the final solution by setting ε_w to equation (44).

In Figure 6 we present the simulated results for velocity u, turbulence kinetic energy k and rate-or-dissipation energy ε. The velocity profile compares well with that obtained by experimental measurement[40] in the near- and far-wall regions. One can observe excellent agreement as well for the k-profile. We present a calculated ε-profile for which no experimental measurements are available. In Figure 6(c) the $k^+ = k/(u^*)^2$ and $\varepsilon^+ = \varepsilon v/(u^*)^4$ profiles in the near-wall zones are presented along with those obtained with the wall functions of equations (23) and (37). One can observe that the wall functions proposed are in agreement with the calculated values in the viscous sublayer ($0 \leqslant y^+ \leqslant 5$) and in the turbulent sublayer defined by $70 \leqslant y^+ \leqslant 100$. However, one notices significant differences in the zone $10 \leqslant y^+ \leqslant 50$, which represents the buffer sublayer and part of the turbulent sublayer. Thus certain discrepancies in calculated results employing the wall functions when mesh points are situated in this zone may be expected.

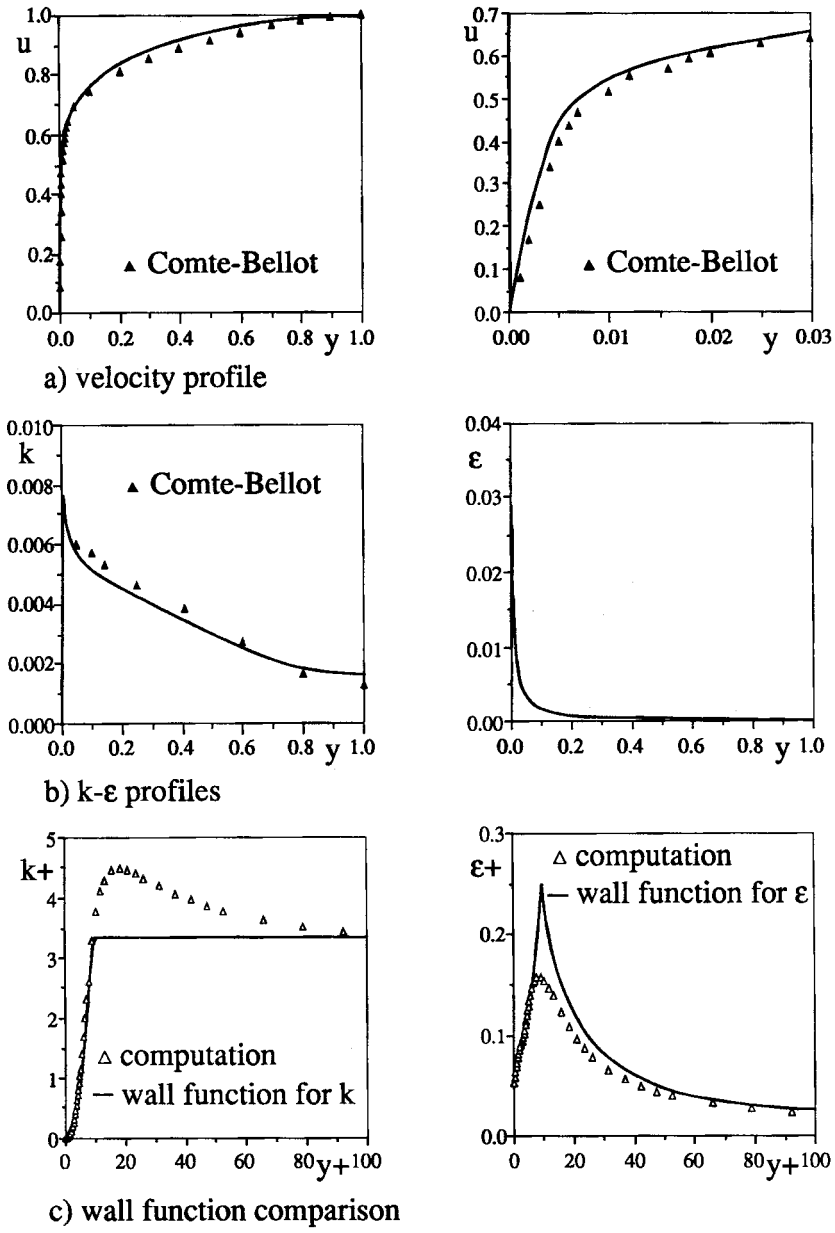

Figure 6. Reference computation

7.2. *Near-wall computations*

We have undertaken 16 computations related to different positions of the mesh boundary in the near-wall zone, i.e.

$$y_{\text{boundary}} = 0{\cdot}0005,\ 0{\cdot}002,\ 0{\cdot}003,\ 0{\cdot}004,\ 0{\cdot}005,\ 0{\cdot}007,\ 0{\cdot}01,\ 0{\cdot}012,\ 0{\cdot}016,\ 0{\cdot}02,\ 0{\cdot}025,\ 0{\cdot}03,\ 0{\cdot}035,\ 0{\cdot}04,\ 0{\cdot}045,\ 0{\cdot}05$$

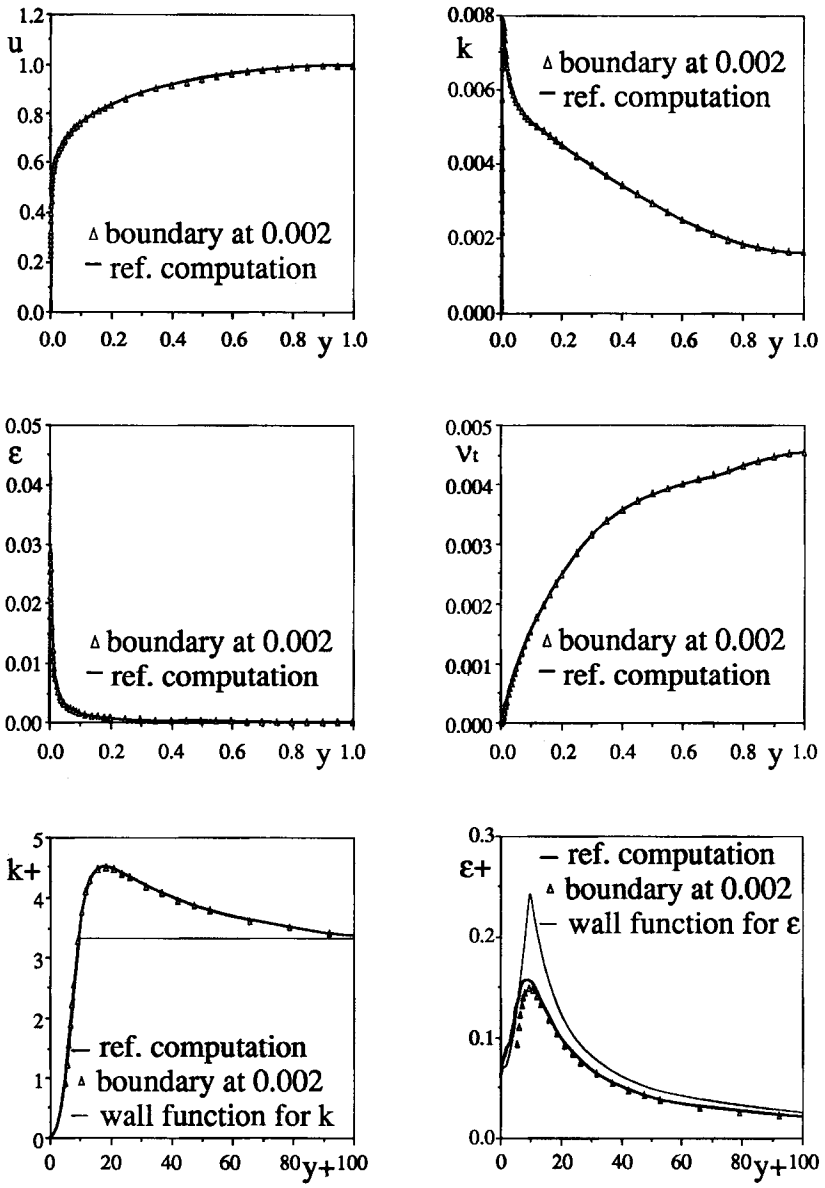

Figure 7. Results with boundary at $y=0{\cdot}002$ (viscous sublayer $y^+=5$)

or

$$y^+ \approx 1, 5, 8, 10, 13, 18, 26, 32, 42, 53, 66, 79, 92, 105, 119, 132.$$

The mesh configuration of the reference computation is so chosen that the element boundaries coincide with the different values of y_{boundary} chosen for the near-wall case studies. For a given value of y_{boundary}, one simply removes the elements situated in $0 \leqslant y \leqslant y_{\text{boundary}}$.

The shear stress τ_w and k–ε boundary conditions on the near-wall boundary points are imposed using the wall functions. In the finite element model we make use of the special four-node boundary elements of Figure 3 to introduce these conditions.

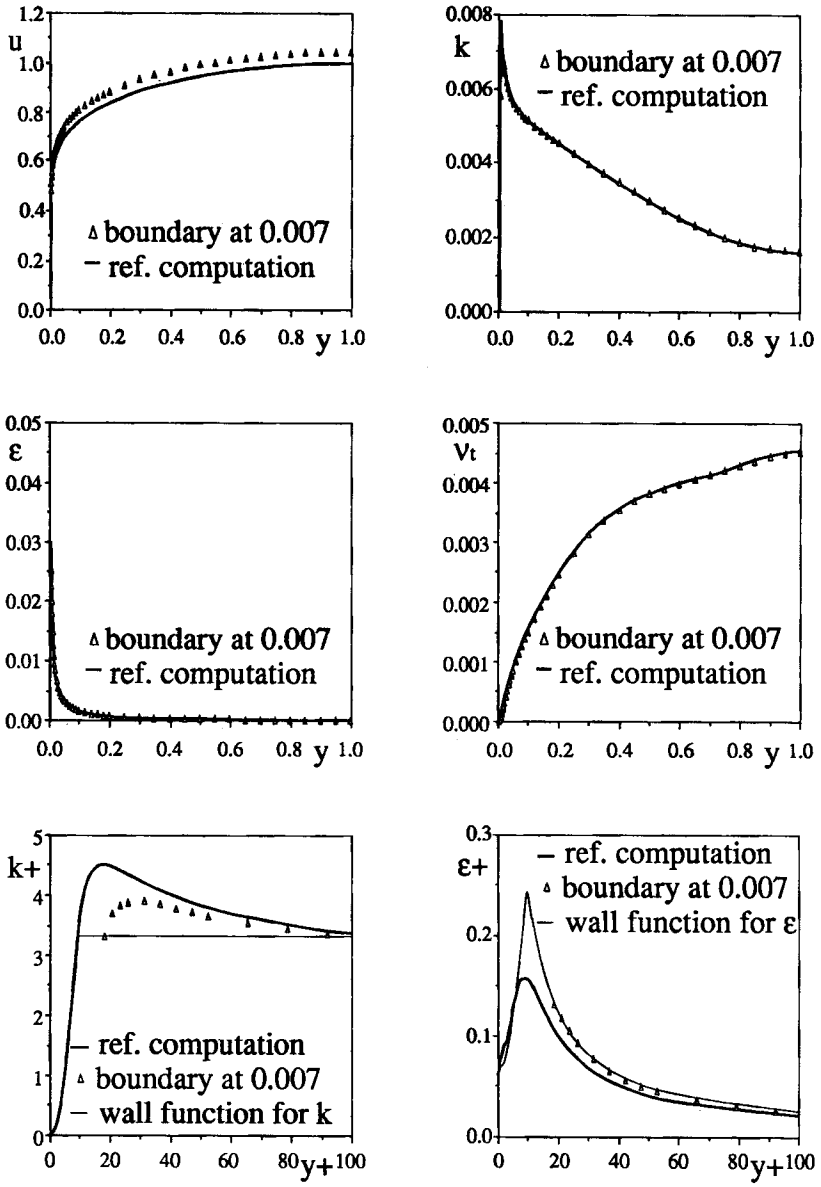

Figure 8. Results with boundary at $y=0{\cdot}007$ (buffer sublayer $y^+=18$)

In order to obtain rapid convergence, the initial solutions for the velocity and k–ε fields are deduced from those obtained with the reference computation. In general the solution converged in 10–15 iterations. In Figures 7–9 the results are presented for three different computations which correspond to three positions of boundary points in the viscous, buffer and turbulent layers. For each case we present the velocity k–ε and eddy viscosity profiles. In the near-wall region the variations in k^+ and ε^+ are plotted against y^+. The results are compared with those obtained with the reference computation. The results for k^+ and ε^+ include comparison with the wall function values.

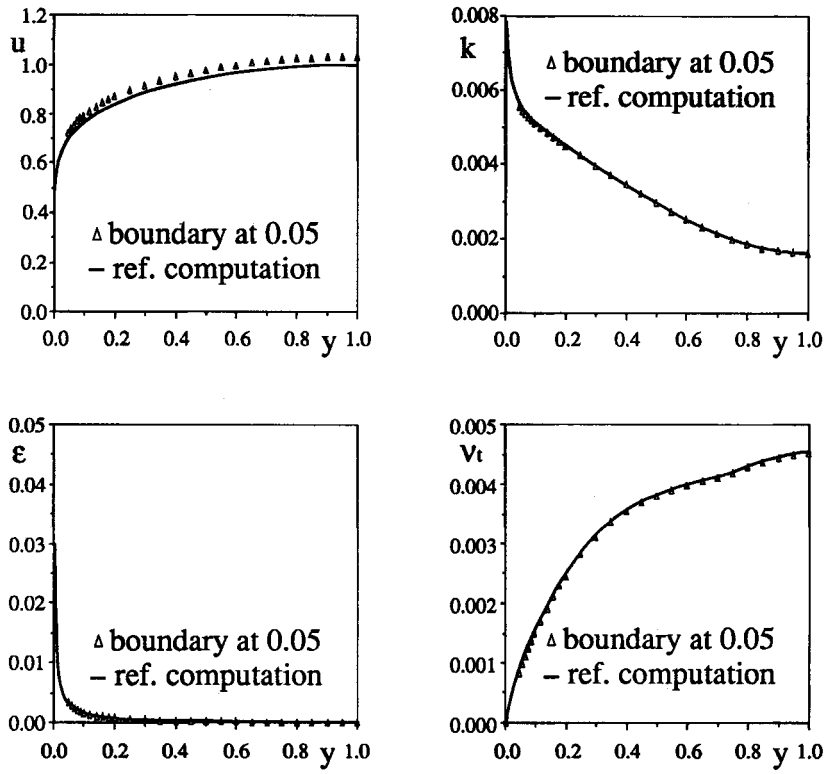

Figure 9. Results with boundary at $y=0{\cdot}05$ (turbulent sublayer $y^+=132$)

Excellent agreement is observed when the mesh boundary is situated in the viscous sublayer ($y=0{\cdot}002$, $y^+\approx 5$). One notices a discrepancy for results obtained with the mesh boundary situated at $y=0{\cdot}007$, which represents the buffer layer. As pointed out in Section 7.1, the difference between the estimated values of k–ε using wall functions and those obtained from the reference computation will lead to certain variations. Moreover, $y=0{\cdot}007$ ($y^+=18$) corresponds to the position which will give the largest discrepancy between the near-wall computation and the reference computation.

For the computation with the boundary situated in the turbulent zone ($y=0{\cdot}05$, $y^+=132$) the results compare well with those obtained by the reference computation.

8. CONCLUSIONS

In this study we have presented an extended k–ε model which is valid in the low-Reynolds-number regions. The main feature of the model is proper choice of weighting functions which make the extension to the wall reliable. The choice of a correct boundary condition for the rate-of-dissipation energy ε is crucial. We have observed that the Chapman and Kuhn condition (equation (33)) is most appropriate.

In order to reduce the computational cost, a set of wall functions is proposed which give the required boundary conditions for τ_w, k and ε for points situated in the viscous, buffer or turbulent sublayer.

The finite element model is based on the standard mixed variational formulation where the incompressibility constraint is penalized. We have employed different types of four-node boundary elements to handle the pressure boundary condition and the boundary conditions on τ_w, k and ε in the near-wall regions. A Newton-type solution method is employed to solve the non-linear equations in a decoupled manner.

The numerical results have been compared with those obtained from experimental measurements for a flow between two plates at $Re = 63\,000$. We have shown that the proposed model with the weighting functions leads to reliable results when the mesh is extended to the wall. Sixteen computations with different mesh positions in the wall regions have shown that the wall functions proposed in this study are well adapted to the near-wall regions.

Numerical experience has shown that the convergence characteristics of the k–ε finite element model are not encouraging. Solving the Navier–Stokes equations poses no problem. We feel that a variant of the Newton-type method is quite acceptable. One may employ GMRES-type[28,41] solvers if necessary. However, there is a need for research effort to develop robust solvers for k–ε finite element models with the mesh boundary situated anywhere in the wall regions. The following comments may be made.

1. Initial estimates for k–ε are important for proper convergence.
2. Appearances of negative values for k and ε are troublesome. Simply flagging them to zero may work in some cases but may not work in other situations.
3. The choice of inflow/outflow conditions for velocity and k–ε is important and requires further investigation.
4. An esoteric use of relaxation factors for velocity and k–ε update needs to be replaced by a well-defined strategy. We feel that the success of a solver is based on elaborating a strategy which is adaptable to different flows without the interference of a researcher.
5. The use of time-marching schemes needs to be explored. The problem of negative k–ε values and choice of relaxation factors will appear anyway.

REFERENCES

1. J. Smagorinsky, 'General circulation experiments with the primitive equations, I: The basic experiment', *Mon. Weather Rev.*, **91**(3), 99–164 (1963).
2. D. K. Lilly, 'On the application of the eddy viscosity concept in the inertial sub-range of turbulence', *NCAR Rep. 123*, 1966.
3. J. W. Deardorff, 'A numerical study of three-dimensional turbulent channel flow at large Reynolds numbers', *J. Fluid Mech.*, **41**, 453–480 (1970).
4. A. Leonard, 'Energy cascade in large eddy simulation of turbulent flows', *Adv. Geophys. A*, **18**, 237–248 (1974).
5. U. Schumann, 'Subgrid scale model for finite difference simulation of turbulent flows in plane channels and annuli', *J. Comput. Phys.*, **18**, 376–404 (1975).
6. R. A. Clark, J. H. Ferziger and W. C. Reynolds, 'Evaluation of subgrid-scale turbulence models using a fully simulated turbulent flow', *Rep. TF-9*, Thermosciences Division, Stanford University, 1977.
7. P. Moin and J. Kim, 'Numerical investigation of turbulent channel flow', *J. Fluid Mech.*, **118**, 341–377 (1982).
8. Y. N. Dakhoul and K. W. Bedford, 'Improved averaging method for turbulent flow simulation. Part I: Theoretical development and application to Burger's transport equation: Part II: Calculation and verification', *Int. j. numer. methods fluids*, **6**, 49–82 (1986).
9. W. K. Yeo, 'A generalized high-pass/low-pass averaging procedure for deriving and solving turbulent flow equations', *Ph.D. Dissertation*, The Ohio State University, Columbus, OH, 1987.
10. O. Reynolds, 'An experimental investigation of the circumstances which determine whether the motion of water shall be direct or sinuous, and the law of resistance in parallel channels', *Phil. Trans. R. Soc. Lond. Ser. A*, **174**, 935–982 (1893).
11. S. A. Monin and A. M. Yaglom, *Statistical Fluid Mechanics*, MIT Press, Boston, MA, 1971.
12. J. Boussinesq, 'Essai sur la théorie des eaux courantes', *Mémo. Acad. Sci. Paris*, **23**, 1–680 (1877).
13. B. E. Launder and D. B. Spalding, 'The numerical computation of turbulent flows', *Comput. Methods Appl. Mech. Eng.*, **3**, 269–289 (1974).

14. P. Broadshaw, *Turbulence*, Springer New York, 1978.
15. W. Rodi, *Turbulence Models and Their Application in Hydraulics: A State of the Art Review*, International Association for Hydraulic Research, Delft, 1980.
16. B. Lakshminarayana, 'Turbulence modelling for complex flows', *AIAA 18th Fluid Dynamics and Plasmadynamics and Lasers Conf.*, Cincinatti, OH, 1985, AIAA, New York.
17. N. Nallasamy, 'Turbulence models and their application to the prediction of internal flows: a review', *Comput. Fluids*, **15**, 151–194 (1987).
18. J. C. Rotta, 'Statisliche Theorie nichthomogener Turbulenz', *Z. Phys.*, **129**, 547–572 (1951).
19. B. J. Dlay and F. H. Harlow, 'Transport equations in turbulence', *Phys. Fluids*, **13**, 2634–2649 (1970).
20. K. Hanjalic and B. E. Launder, 'A Reynolds stress model of turbulence and its applications to thin shear flows', *J. Fluid Mech.*, **52**, 609–638 (1972).
21. B. E. Launder, G. J. Reece and W. Rodi, 'Progress in the development of a Reynolds stress turbulence closure', *J. Fluid Mech.*, **68**, 538–566 (1975).
22. K. Hanjalic and B. E. Launder, 'Contribution towards a Reynolds stress closure for low-Reynolds number turbulence', *J. Fluid Mech.*, **74**, 593–610 (1976).
23. B. E. Launder, Second-moment closure and its use in modelling turbulent industrial flows', *Int. j. numer. methods fluids*, **9**, 963–985 (1989).
24. H. Schlichting, *Boundary Layer Theory*, McGraw-Hill, New York, 1979.
25. J. Happel and H. Brenner, *Low Reynolds Number Hydrodynamics*, Kluwer, Dordrecht, 1986.
26. H. Tennekes and J. L. Lumley, *A First Course in Turbulence*, MIT Press, Boston, MA, 1972.
27. W. P. Jones and B. E. Launder, 'The prediction of laminarization with a two-equation model of turbulence', *Int. J. Heat Mass Transfer*, **15**, 301–314 (1972).
28. O. Pironneau, *Méthodes des Éléments Finis pour les Fluides*, Masson, Paris, 1988.
29. B. E. Launder and B. I. Sharma, 'Application of the energy-dissipation model of turbulence to the calculation of flow near a spinning disc', *Lett. Heat Mass Transfer*, **1**, 131–138 (1974).
30. G. H. Hoffman, 'Improved form of the low Reynolds numbers k–ε turbulence model', *Phys. Fluids*, **18**, 309–312 (1975).
31. W. C. Reynolds, 'Computation of turbulent flows', *Ann. Rev. Fluid Mech.*, **8**, 183–208 (1976).
32. S. Hassid and M. Poreh, 'A turbulent energy dissipation model for flows with drag reduction', *J. Fluids Eng.*, **100**, 107–112 (1978).
33. C. K. G. Lam and K. Bremhorst, 'A modified form of the k–ε model for predicting wall turbulence', *J. Fluids Eng.*, **103**, 457–460 (1981).
34. K. Y. Chien, 'Predictions of channel and boundary-layer flows with a low Reynolds number turbulence model', *AIAA J.*, **20**, 33–38 (1982).
35. C. Patel, W. Rodi and G. Schewerer, 'Turbulence models for near-wall an low Reynolds number flows: a review', *AIAA J.*, **23**, 1308–1319 (1985).
36. E. W. Miner, T. F. Swean Jr., R. A. Handler and R. I. Leighton, 'Examination of wall damping for the k–ε turbulence model using direct simulations of turbulent channel flow', *Int. j. numer. methods fluids*, **12**, 609–624 (1991).
37. D. R. Chapman and G. D. Kuhn, 'Navier–Stokes computations of viscous sublayer flow and the limiting behaviour of turbulence near a wall', *AIAA 7th Computational Fluid Dynamics Conf.*, Cincinatti, OH, 1985, AIAA, New York.
38. M. Jaeger, 'Simulation numérique d'écoulements turbulents incompressibles et isothermes de fluides newtoniens par éléments finis tridimensionnels', *Thèse de Doctorat*, Université de Technologie de Compiègne, 1990.
39. G. Dhatt and G. Hubert, 'A study of penalty elements for incompressible laminar flows', *Int. j. numer. methods fluids*, **6**, 1–19 (1986).
40. G. Comte-Bellot, 'Contribution à l'étude de la turbulence de conduite', *Thèse de Docteur ès Sciences*, 1963.
41. Y. Saad and M. H. Schultz, 'GMRES: a generalized minimal residual algorithm for solving nonsymmetric linear systems', *SIAM J. Sic. Stat. Comput.*, **7**, 856–869 (1986).